A Novel Bistatic Scattering Matrix Measurement Technique Using a Monostatic Radar

Kamal Sarabandi, *Senior Member, IEEE*, and Adib Nashashibi, *Member, IEEE*

Abstract—**In this paper, we present a new technique for measuring the bistatic scattering matrix of point targets using a monostatic radar. In this technique, the complexity of the traditional bistatic measurement setup and difficulties in retaining the phase coherence between the transmitter and the receiver are circumvented completely. The bistatic measurement is performed using a wideband, polarimetric, monostatic radar in conjunction with a rotatable ground plane positioned behind the target. Assuming that the distance between the target and the ground plane is larger than the radar resolution, the desired bistatic response (image contribution) can be isolated from the unwanted backscatter. Noting that the radar operates in the backscatter mode and using the reciprocity theorem, it is shown that the measured cross-polarized responses (σ_{vh} and σ_{hv}) cannot be determined uniquely. To rectify this problem, additional independent measurements are required. Additional equations for characterizing the cross-polarized components are obtained by placing an anisotropic lossless slab over the perfectly conducting flat surface. The validity and accuracy of the new bistatic measurement technique is demonstrated by measuring a number of point targets with known theoretical bistatic responses. Also, a new approach for determining the effective dielectric constant of dense random media based on the new bistatic measurement technique is developed.**

I. Introduction

TRADITIONALLY, polarimetric bistatic radar cross section (RCS) measurements of point targets have been conducted using two disjoint dual-polarized antennas [1]. In this method, the transmitter and the target are often kept fixed and the receiver is moved on the surface of a sphere, having the target at its center, to measure the bistatic RCS at different bistatic angles (see Fig. 1). The difficulties associated with the traditional bistatic measurement technique can be categorized into three groups: 1) A complicated experimental setup is required in which the scattered wave from the supporting structure must be minimized, 2) phase coherence between the transmitter and the receiver must be maintained as the microwave cables move with the receiving antenna, and 3) a complicated calibration procedure is needed to keep track of the orientation of the antennas with respect to the target.

The measurement technique considered in this paper has a significant impact on the modeling of electromagnetic scattering from random media. Existing theoretical models for random media may be categorized into two modeling approaches: 1) Continuous, such as the Born approximation, and 2) discrete, such as radiative transfer. In either of these two approaches, the characterization of both the effective propagation constant of the mean field and the incoherent scattered power in the random medium are of great importance. For example, for tenuous random media, where the radiative transfer theory has been widely used, knowledge of the bistatic scattering characteristics of individual scatterers comprising the medium are essential for estimating the extinction and phase function of that medium directly. Also, bistatic scattering measurements can be used to verify the proposed theoretical models for individual scatterers [2]–[3]. For dense random media—analytical models, such as the effective field approximation (EFA) and the quasicrystalline approximation with coherent potential (QCA-CP) [4]—are widely used to compute the effective propagation constant.

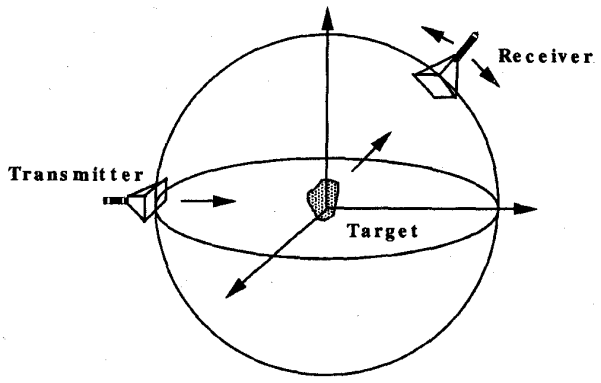

Fig. 1. Experimental setup for the traditional bistatic scattering matrix measurement technique.

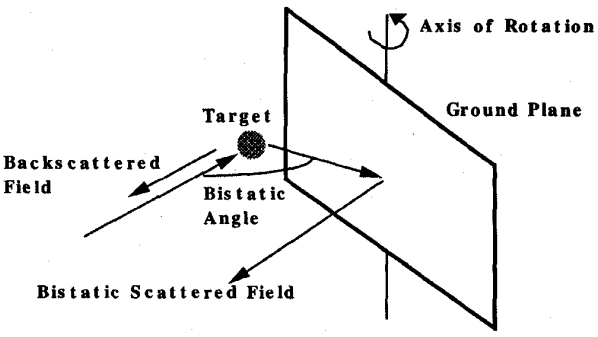

Fig. 2. Experimental setup for the new bistatic scattering matrix measurement technique.

Manuscript received January 28, 1995; revised June 8, 1995.

The authors are with The Radiation Laboratory, Department of Electrical Engineering and Computer Science, University of Michigan, Ann Arbor, MI 48109-2122 USA.

Publisher Item Identifier S 0018-926X(96)00616-3.

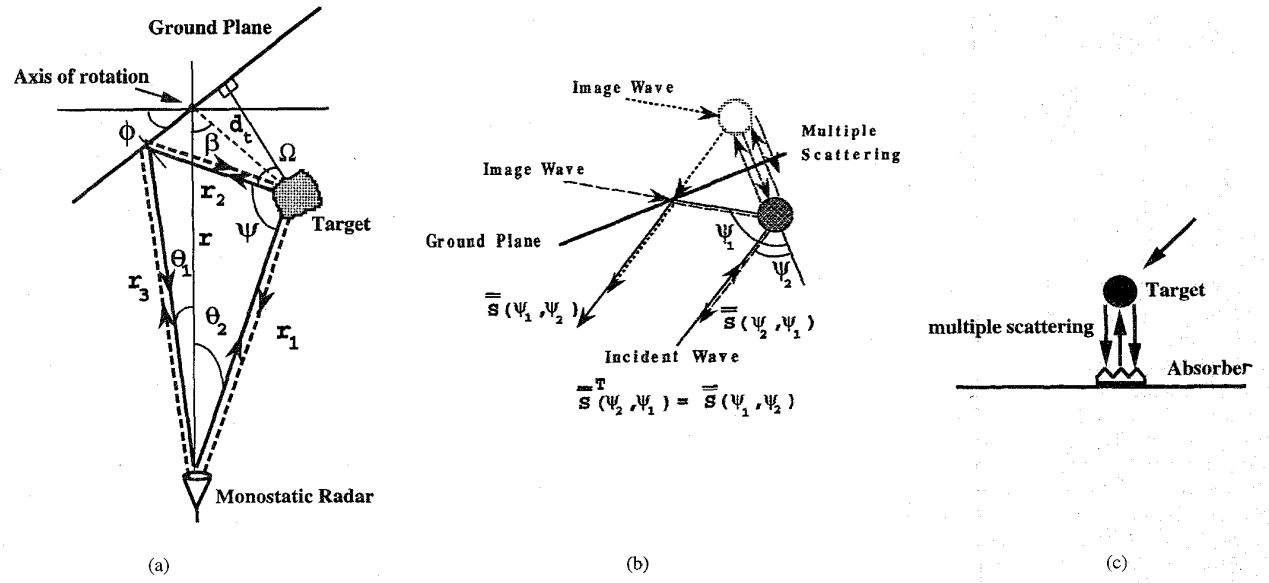

(a) (b) (c)

Fig. 3. Scattering configuration in the prescence of a ground plane, the new experimental setup illustrating (a) top view of the measurement setup, (b) the interactions of the image waves with the target and its image, and (c) application of a radar absorber to minimize the effect of multiple scattering between the target and its image.

Accurate measurements of the effective propagation constant (K) can be used for establishing the range of validity of the existing analytical models. Direct measurements can also be used in the developement of empirical models for the effective propagation constant. Motivated by the need for an experimental procedure for the measurement of the effective propagation constant of dense random media, the development of a convenient technique for measuring the bistatic scattering matrix of point targets is considered. Basically, the bistatic scattering from a cluster of constituent particles of a random medium confined in a spherical or cylindrical volume will be measured. The coherent and incoherent components of the scattered fields can be separated using many independent measurements of the cluster for given incident and bistatic directions. Independent radar measurements are obtained by rotating the cluster of particles around its axis of symmetry, perpendicular to the direction of propagation, and/or randomizing the particles within the confining volume. The coherent scattered wave (mean field) is proportional to the effective dielectric constant (or equivalently, the effective propagation constant) of the medium, and the incoherent scattered power is proportional to the phase function of the random medium.

In the following section, a new approach for measuring the bistatic scattering matrix of point targets is described. In this technique, a polarimetric monostatic radar in conjunction with a ground plane are used for the bistatic measurements and it is shown that the new technique circumvents the drawbacks of the traditional measurement technique. In Section III, a system distortion model and an appropriate calibration procedure are developed for the proposed measurement setup. To fully characterize the bistatic scattering matrix, that is, to resolve the cross-polarized components, radar measurements must be repeated after loading the ground plane with an anisotropic layer. Two methods for designing the anisotropic dielectric layer required for loading the ground plane are discussed in Section IV. In Section V, experimental data for canonical targets are presented to verify the accuracy of the new bistatic scattering matrix measurement technique. Also, the effective dielectric constant of a dense random medium (sand with a volume fraction of 0.6) is estimated to demonstrate the feasibility of the proposed technique in characterizing the fundamental scattering properties of random media.

II. Bistatic Scattering Measurement Technique

In this technique, a wideband, polarimetric, monostatic radar, in conjunction with a rotatable perfectly conducting plane, is used to measure the bistatic scattering matrix of a target. The simplified bistatic RCS measurement setup is shown in Fig 2. In this measurement configuration, the bistatic measurement can be performed in one scattering plane at a time. To change the scattering plane, the orientation of the target, with respect to the radar system, can be adjusted appropriately. In this method, the role of the ground plane is to excite the image wave (see Fig. 3) whose interactions with the target and its image produce the desired bistatic term. Primarily, there are three major scattering components that contribute to the signal received by the radar. However, their responses arrive at the antenna at different times. The first component is due to the direct backscatter from the target which arrives at the antenna with a delay time of $2r_1/c$, where c is the speed of light [see Fig. 3(a)]. The second component, which in turn is comprised of two subcomponents, is due to the bistatic scattering from the target being illuminated by the image wave [the long-dotted line in Fig. 3(b)] and its complementary which is the bistatic scattering from the image target illuminated by the image wave [the short-dotted line in Fig. 3(b)]. These two subcomponents arrive at the antenna with a delay time of $(r_1 + r_2 + r_3)/c$ [see Fig. 3(a)]. The third component is due to the reflected backscattering of the image wave from the target through the

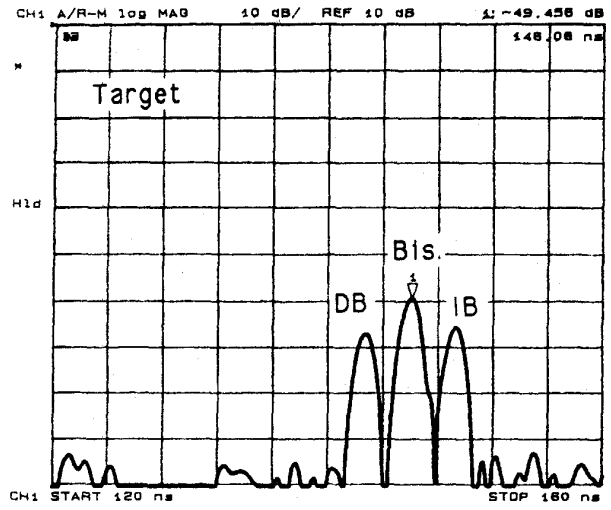

(a)

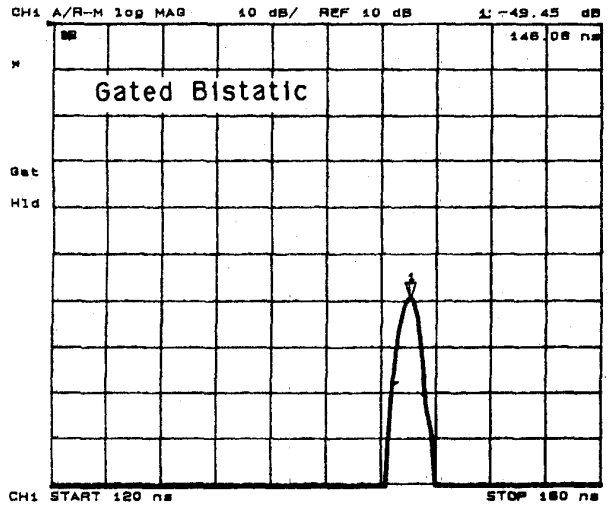

(b)

Fig. 4. A time-domain response of a target in the presence of a ground plane (a) the three major components of the measured signal and (b) the gated bistatic component.

ground plane, which arrives at the antenna with a delay time of $2(r_2 + r_3)/c$. There are many higher order scattering terms which are the result of multiple scattering between the target and its image. The contribution of these terms to the overall backscattered signal is negligible if the distance between the target and the ground plane is much larger than the wavelength [5]. Experimentally, the effect of these terms can be reduced even further by placing an absorber on the ground plane between the target and its image, as illustrated in Fig. 3(c). By choosing the distance between the target and the ground plane to be larger than the radar resolution, all components of the measured backscattered signal can be resolved and collected separately. For example, the magnitude of the total backscattered response from a sphere, measured in an anechoic chamber using a network analyzer-based monostatic radar, is plotted as a function of time and shown in Fig. 4(a). To eliminate the undesired backscatter from the edges of the

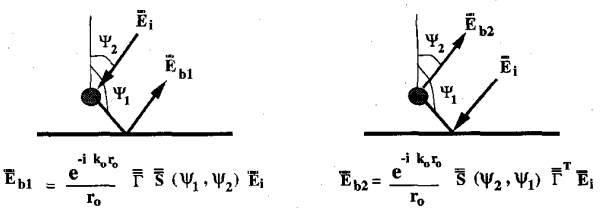

Fig. 5. The two complementary subcomponents of the bistatic response.

ground plane, the backscatter response of the ground plane alone (without the target) was subtracted coherently from the backscatter response of the ground plane and the target. The first peak in Fig. 4(a) corresponds to the direct backscatter component (DB), while the second peak corresponds to the total bistatic component (BIS) (the two complementary subcomponents), and the third peak corresponds to the indirect backscatter component (IB). Since the three components of the backscatter response arrive at the antenna at different times, the BIS component can be isolated from the others using the range gating capability of the network analyzer. The gated bistatic response is shown in Fig. 4(b).

The second component of the scattered signal contains the desired bistatic scattering response of the target. By defining a set of orthogonal directions $(\hat{v}, \hat{h})$ in a plane perpendicular to the direction of propagation, the bistatic scattered signal $\overline{\boldsymbol{E}}_{\boldsymbol{b}}$ can be related to the incident signal through the total measured bistatic scattering matrix, i.e.,

$$\overline{\boldsymbol{E}}_{\boldsymbol{b}} = \frac{e^{-ik_o r_o}}{r_o} \overline{\overline{\boldsymbol{S}}}_{\boldsymbol{b}} \, \overline{\boldsymbol{E}}_{\boldsymbol{i}} \tag{1}$$

where k_o is the free space propagation constant and $\overline{\overline{\boldsymbol{S}}}_{\boldsymbol{b}}$ is the total measured bistatic scattering matrix. The total bistatic scattering matrix is a function of the desired scattering matrices of the two complementary subcomponents, $\overline{\overline{\boldsymbol{S}}}(\Psi_1, \Psi_2)$ and $\overline{\overline{\boldsymbol{S}}}(\Psi_2, \Psi_1)$, and the reflectivity matrix of the ground plane $(\overline{\overline{\boldsymbol{\Gamma}}}(\pi - \Psi_1))$, as shown in Fig. 5. Here, $\Psi_1$and Ψ_2 are the bistatic angles defining the incident and scattering directions. In the most general case corresponding to an anisotropic surface, $\overline{\overline{\boldsymbol{\Gamma}}}(\pi - \Psi_1)$ is a 2×2 matrix whose entries are the reflection coefficients of the ground plane. Since the two subcomponents (bistatic terms) arrive at the same time, they cannot be resolved in the time domain and the target's bistatic scattering matrices $\overline{\overline{\boldsymbol{S}}}(\Psi_1, \Psi_2)$ and $\overline{\overline{\boldsymbol{S}}}(\Psi_2, \Psi_1)$ cannot be uniquely determined. The reciprocity theorem mandates that $\overline{\overline{\boldsymbol{S}}}(\Psi_1, \Psi_2) = \overline{\overline{\boldsymbol{S}}}^{\boldsymbol{T}}(\Psi_2, \Psi_1)$ and $\overline{\overline{\boldsymbol{\Gamma}}}(\pi - \Psi_1) = \overline{\overline{\boldsymbol{\Gamma}}}^{\boldsymbol{T}}(\pi - \Psi_1)$. Thus, the total measured bistatic scattering matrix given by

$$\overline{\overline{\boldsymbol{S}}}_{\boldsymbol{b}} = \frac{e^{-ik_o r_o}}{r_o} (\overline{\overline{\boldsymbol{\Gamma}}}(\pi - \Psi_1) \overline{\overline{\boldsymbol{S}}}(\Psi_1, \Psi_2) + [\overline{\overline{\boldsymbol{\Gamma}}}(\pi - \Psi_1) \overline{\overline{\boldsymbol{S}}}(\Psi_1, \Psi_2)]^{\boldsymbol{T}}) \tag{2}$$

is symmetric. This poses a difficulty in characterizing the desired bistatic scattering matrix $\overline{\overline{\boldsymbol{S}}}$ in that there are only three independent equations for the four unknown elements of the bistatic scattering matrix $\overline{\overline{\boldsymbol{S}}}$. To resolve this ambiguity, an additional measurement is needed in which the target's

orientation and position remain the same, while the reflective property of the ground plane is changed. This is achieved by placing an anisotropic lossless layer over the perfectly conducting plane.

In summary, the measurement procedure involves three steps, starting with positioning the point target in front of the ground plane at an appropriate distance. Then the ground plane is rotated to the desired bistatic angle and the second component of the backscattered signal is measured. Finally, the second step is repeated for the same bistatic angles after attaching the anisotropic slab to the ground plane. Care must be taken so that the position of the ground plane is not disturbed.

III. Calibration Technique

Characterization of measurement accuracy and precision are the critical elements of any meaningful measurement procedure. Imperfections in the radar system components, such as antenna polarization contamination (coupling between the orthogonal polarization ports of the antenna) and channel imbalances (variations in magnitude and phase of the system transfer function for different ports of the receiver), can lead to serious errors in the measured scattering matrix. The role of a calibration procedure is then to remove the systematic errors from the measured target response. In this section, the imperfections of the monostatic radar system is modeled mathematically and a procedure for determining the system distortion parameters is outlined. Basically, a metallic sphere is used as the external calibration target and the radar distortions are obtained using the mathematical model.

A. System Distortion Model

Depending on the distance between the target and the radar, the direction of the transmitted and received rays, with respect to the antenna's boresight, can be quite different. The complementary bistatic terms propagate along directions defined by angles θ_1 and θ_2,, as shown in Fig. 3(a). These rays experience different transfer functions since the systematic errors vary over the mainlobe of the antenna. Thus, it is important to first, characterize the systematic errors of the radar antenna over its mainlobe and construct a system distortion model; and second, remove these errors from the measured bistatic response using an appropriate calibration procedure. The proposed system distortion model is an extension of the model developed for single-antenna polarimetric radars [6]. In this paper [6], it is shown that the measured scattering matrix ($\overline{\overline{\boldsymbol{M}}}$) of a point target in terms of the actual scattering matrix and the radar distortions can be obtained from

$$\overline{\overline{\boldsymbol{M}}} = \frac{e^{-2ikr}}{r^2}\overline{\overline{\boldsymbol{R}}}\,\overline{\overline{\boldsymbol{D}}}(\theta_o)\overline{\overline{\boldsymbol{C}}}(\theta_o)\overline{\overline{\boldsymbol{S}}}\,\overline{\overline{\boldsymbol{C}}}(\theta_o)\overline{\overline{\boldsymbol{D}}}(\theta_o)\overline{\overline{\boldsymbol{T}}} \tag{3}$$

where θ_o is an angle representing the position of the target with respect to the antenna. In (3), $\overline{\overline{\boldsymbol{R}}}, \overline{\overline{\boldsymbol{T}}}, \overline{\overline{\boldsymbol{C}}}$, and $\overline{\overline{\boldsymbol{D}}}$ are 2×2 matrices representing the radar distortions and are given by

$$\overline{\overline{\boldsymbol{R}}} = \begin{bmatrix} R_v & 0 \\ 0 & R_h \end{bmatrix}, \qquad \overline{\overline{\boldsymbol{T}}} = \begin{bmatrix} T_v & 0 \\ 0 & T_h \end{bmatrix}$$
$$\overline{\overline{\boldsymbol{C}}} = \begin{bmatrix} 1 & c \\ c & 1 \end{bmatrix}, \qquad \overline{\overline{\boldsymbol{D}}} = \begin{bmatrix} d_1 & 0 \\ 0 & d_2 \end{bmatrix}.$$

Here, the parameters (T_v, T_h) and (R_v, R_h) are the channel imbalances due to the active components in the transmit and receive branches of the radar, respectively, $c(\theta_o)$ is the antenna cross-talk factor, and $(d_1(\theta_o), d_2(\theta_o))$ are the channel imbalances of the antenna system. It should be noted that the channel imbalance parameters (T_v, T_h) and (R_v, R_h) are independent of the target angle θ_o. As mentioned before, the measured bistatic scattering matrix is comprised of two complementary components that arrive at the radar simultaneously and thus are inseparable in the time domain. These components are designated by the solid and dotted lines in Fig. 3(a). The system distortion model described in (3) is modified to include the possible differences in the radar distortion parameters for the transmit and receive rays. Thus, the distortion model for the second component of the measured radar response is given by

$$\overline{\overline{\boldsymbol{M}}} = \frac{e^{-ik(r_1+r_2+r_3)}}{r_1(r_2+r_3)}\overline{\overline{\boldsymbol{R}}}\{\overline{\overline{\boldsymbol{D}}}(\theta_2)\overline{\overline{\boldsymbol{C}}}(\theta_2)\overline{\overline{\boldsymbol{S}}}^{\boldsymbol{T}}(\psi_1,\psi_2)\overline{\overline{\boldsymbol{I}}}^{\boldsymbol{T}}\overline{\overline{\boldsymbol{C}}}(\theta_1) \cdot \overline{\overline{\boldsymbol{D}}}(\theta_1) + \overline{\overline{\boldsymbol{D}}}(\theta_1)\overline{\overline{\boldsymbol{C}}}(\theta_1)\overline{\overline{\boldsymbol{I}}}\,\overline{\overline{\boldsymbol{S}}}(\psi_1,\psi_2)\overline{\overline{\boldsymbol{C}}}(\theta_2)\overline{\overline{\boldsymbol{D}}}(\theta_2)\}\overline{\overline{\boldsymbol{T}}} \tag{4}$$

The first term in the bracket corresponds to the bistatic scattering of the target when illuminated by the image wave and the second term corresponds to the bistatic scattering of the image target when illuminated by the image wave. It should be noted that in the derivation of (4), the reciprocity theorem has been used to express the bistatic scattering matrix of the target when illuminated by the image wave $\overline{\overline{\boldsymbol{S}}}(\psi_2,\psi_1)$ in terms of the scattering matrix of the target when illuminated by the incident wave $\overline{\overline{\boldsymbol{S}}}(\psi_1,\psi_2)(\overline{\overline{\boldsymbol{S}}}(\psi_2,\psi_1) = \overline{\overline{\boldsymbol{S}}}^{T}(\psi_1,\psi_2))$. Once the radar distortion parameters are determined, the elements of the bistatic scattering matrix $\overline{\overline{\boldsymbol{S}}}$ can be computed by inverting (4). These unknown terms can be determined by measuring the polarimetric response of a metallic sphere in the backscattering configuration over the entire mainlobe of the antenna (no ground plane). By applying the single target calibration technique (STCT) [6], the cross-talk factors and channel imbalances can be determined from the polarimetric sphere measurements ($\overline{\overline{\boldsymbol{M}}}^{s}$) and are given by

$$c(\theta_o) = \pm\frac{1}{\sqrt{a}}(1-\sqrt{1-a}), \qquad a = \frac{m^s_{vh}m^s_{hv}}{m^s_{vv}m^s_{hh}}$$
$$\sqrt{R_vT_v}\,d_1(\theta_o) = r_s e^{ikr_s}\sqrt{\frac{m^s_{vv}/s_o}{1+c^2(\theta_o)}}$$
$$\sqrt{R_hT_h}\,d_2(\theta_o) = r_s e^{ikr_s}\sqrt{\frac{m^s_{hh}/s_o}{1+c^2(\theta_o)}}$$
$$\sqrt{\frac{R_vT_h}{R_hT_v}} = \sqrt{\frac{m^s_{vh}}{m^s_{hv}}} \tag{5}$$

In (5), the superscript s refers to the measured sphere response, s_o is the theoretical backscattering amplitude of the metallic sphere, and θ_o can be either θ_1 or θ_2. It should be noted that the antenna's distortion parameters (c, d_1, and d_2) are time invariant and therefore, the elaborate backscatter measurement of the metallic sphere over the entire mainlobe of the antenna need to be performed only once. However, elements of $\overline{\overline{\boldsymbol{R}}}$ and

$\overline{\overline{T}}$ which are influenced by the active elements of the radar must be characterized often. This can be done by measuring a sphere positioned at the boresight of the antenna noting that the elements of $\overline{\overline{R}}$ and $\overline{\overline{T}}$ are independent of the target angle θ_o. Once the distortion parameters at boresight are determined, the expressions given by (5) must be modified by the following factors in order to update the distortion parameters over the entire mainlobe

$$\alpha_1 = \frac{(\sqrt{R_v' T_v'}\, d_1(0°))}{(\sqrt{R_v T_v}\, d_1(0°))}, \qquad \alpha_2 = \frac{(\sqrt{R_h' T_h'}\, d_2(0°))}{(\sqrt{R_h T_h}\, d_2(0°))},$$
$$\alpha_3 = \sqrt{\frac{R_v' T_h'}{R_h' T_v'}} \Bigg/ \sqrt{\frac{R_v T_h}{R_h T_v}}$$

where the primed parameters (R_v', R_h', T_v', T_h') correspond to the last sphere measurement at boresight.

For the sake of completeness, expressions for r_1, r_2, r_3, θ_1, θ_2, and Ψ in terms of the physical setup parameters r, β, d_t, and ϕ, as defined in Fig. 3(a), are provided below

$$r_1 = \sqrt{d_t^2 + r^2 - 2\, d_t r \cos\beta},$$
$$\theta_2 = \sin^{-1}\left[\frac{d_t}{r_1}\sin\beta\right],$$
$$(r_2 + r_3) = \sqrt{(2x)^2 + r_1^2 - 4x r_1 \cos(\pi - \theta_2 - \phi)}$$
$$\theta_1 = -\theta_2 + \sin^{-1}\left[\frac{2x}{(r_2 + r_3)}\sin(\pi - \theta_2 - \phi)\right]$$
$$\Omega = \sin^{-1}\left[\frac{r_1}{(r_2 + r_3)}\sin(\pi - \theta_2 - \phi)\right]$$
$$r_2 = \frac{x}{\cos\Omega}$$
$$\Psi = \pi - (\theta_1 + \theta_2) - 2\Omega$$

where $x = d_t \cos(\phi - \beta)$. Refering to Fig. 3(a), r is the distance between the antenna and the axis of rotation of the ground plane, ϕ denotes the rotation angle of the ground plane, and β and d_t specify the target's position relative to the ground plane. It is noted that the bistatic angle (Ψ) and the direction of propagation of the bistatic response (θ_1) can be computed in terms of the rotation angle of the ground plane (ϕ).

B. Calibration Procedure

Following simple algabraic manipulations, (4) can be cast into a matrix equation of the following form

$$\overline{\overline{A}}\,\overline{x} = \overline{b} \tag{6}$$

where

$$\overline{b} = [m_{vv}, m_{hh}, m_{vh}, m_{hv}]^T, \overline{x} = [S_{vv}, S_{hh}, S_{vh}, S_{hv}]^T$$

and $\overline{\overline{A}}$ is a 4×4 matrix whose elements are a function of the radar distortion parameters and the elements of $\overline{\overline{\Gamma}}$. Having determined the elements of $\overline{\overline{A}}$ from the external calibration, it seems, the elements of the bistatic scattering matrix can be obtained by inverting (6). However, the last two rows of (6) are linearly dependent and in effect only three linearly independent equations are available. Therefore, one of the dependent equations in (6) must be replaced by another independent equation acquired by repeating the experiment after loading the ground plane with an anisotropic dielectric layer. It should be noted that the second bistatic measurement (with loaded ground plane) is not necessary for targets that do not depolarize $(S_{vh} = S_{hv} = 0)$, such as spheres and vertical and horizontal cylinders. In this case, the linear system of equations in (6) reduces to two independent equations for the two unknowns (S_{vv}, S_{hh}). After some algabraic manipulations, it can be shown that

$$S_{vv} = \frac{z_{vv} - c(\theta_1)c(\theta_2)z_{hh}}{\Gamma_v(1 - c^2(\theta_1)c^2(\theta_2))}$$
$$S_{hh} = \frac{z_{hh} - c(\theta_1)c(\theta_2)z_{vv}}{\Gamma_h(1 - c^2(\theta_1)c^2(\theta_2))} \tag{7}$$

where

$$z_{vv} = \frac{e^{ik(r_1+r_2+r_3)} r_1(r_2 + r_3)}{2R_v T_v\, d_1(\theta_1)\, d_1(\theta_2)} m_{vv}$$
$$= \Gamma_v S_{vv} + \Gamma_h c(\theta_1)c(\theta_2) S_{hh}$$
$$z_{hh} = \frac{e^{ik(r_1+r_2+r_3)} r_1(r_2 + r_3)}{2R_h T_h\, d_2(\theta_1)\, d_2(\theta_2)} m_{hh}$$
$$= \Gamma_h S_{hh} + \Gamma_v c(\theta_1)c(\theta_2) S_{vv}. \tag{8}$$

IV. Design of an Anisotropic Surface

To acquire an additional independent measurement to resolve the ambiguity in the measurement of the cross-polarized components, use of an anisotropic dielectric slab to modify the reflection matrix $\overline{\overline{\Gamma}}$ is required. Since the magnitude of the second component of the received signal (the bistatic term) is proportional to the reflection coefficient, the magnitude of the reflection coefficient of the surface must be chosen as high as possible to retain the system sensitivity. Therefore, an anisotropic surface with reflection coefficients having magnitude of unity, similar to those of the perfectly conducting plane, and phases that are very different from those of the ground plane are of interest. Two types of surfaces are considered in this paper to accomplish this task: 1) Loading the ground plane by a periodic corrugated dielectric slab, and 2) loading the ground plane by dielectric loaded periodic strips. If lossless dielectric materials are used, the magnitude of the reflection coefficients will be unity.

A. Periodic Corrugated Dielectric Slab

The proposed one-dimensional periodic surface is shown in Fig. 6(a). It has been demonstrated that a periodic corrugated dielectric layer can be simulated by an anisotropic dielectric layer of equal thickness when the period is small compared to the wavelength [7]. The tensor elements of the equivalent anisotropic layer are given in terms of the permittivity (ϵ), the period of surface corrugation (L), and the width of the corrugation (d). In the low frequency regime, where $L < 0.2\lambda$, the tensor elements are given by

$$\epsilon_y = \epsilon_z = 1 + (\epsilon - 1)\frac{d}{L}$$
$$\epsilon_x = \frac{\epsilon}{\epsilon(1 - d/L) + d/L}. \tag{9}$$

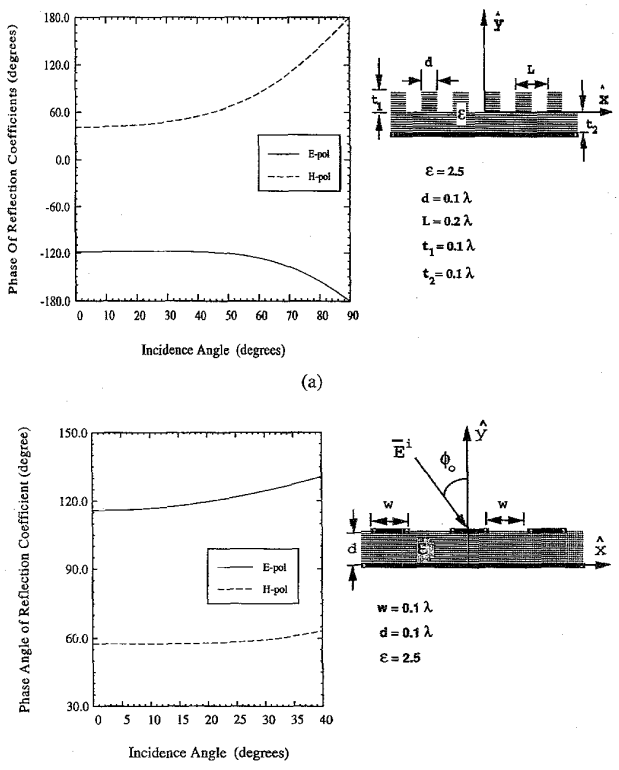

Fig. 6. Phases of the reflection coefficients for (a) periodic corrugated dielectric slab and (b) dielectric loaded periodic strips as functions of the incidence angle.

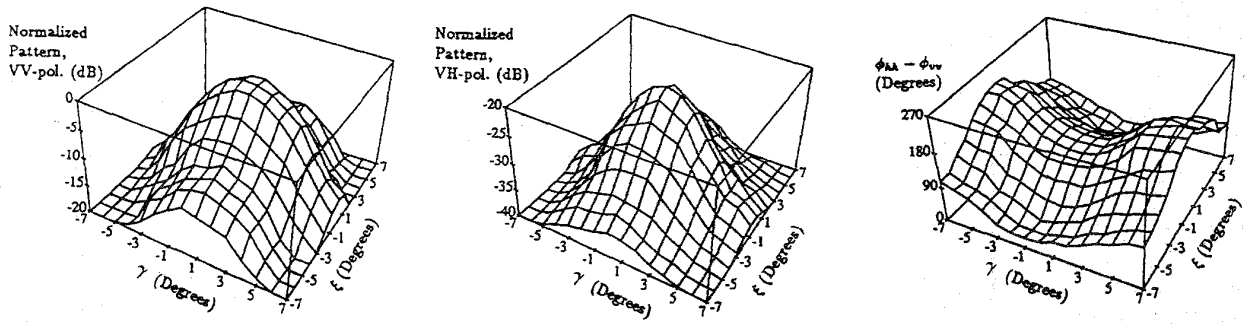

Fig. 7. Measured backscattered response from a sphere over the entire mainlobe of the monostatic radar.

The reflection coefficients of the stratified loaded ground plane can easily be computed [7]. The higher order Bragg modes decay exponentially away from the surface in the low-frequency regime ($L < 0.5\lambda$), thus, the target must be placed far enough from the surface to avoid coupling with the higher order Bragg modes. By appropriately choosing the permittivity of the dielectric, the width, period, and depth of the corrugated layer, the desired phase-difference between the reflection coefficients can be achieved. For example, the phases of the reflection coefficients as functions of the incidence angle when $\epsilon = 2.5, d = 0.1\lambda, L = 0.2\lambda, t_1 = 0.1\lambda$, and $t_2 = 0.1\lambda$ at 9.5 GHz are shown in Fig. 6(a).

B. Dielectric Loaded Periodic Strips

The surface with dielectric loaded periodic strips also behaves as an anisotropic layer and is shown in Fig. 6(b). In this structure, perfectly conducting strips of width w are periodically aligned over a dielectric substrate with permittivity ϵ and thickness d backed by a ground plane. The scattered plane waves can be computed from

$$\overline{E}^s(x,y) = \int_{-w/2}^{w/2} \overline{\overline{G}}^p(x,x') \cdot \overline{J}(x')\, dx' \qquad (10)$$

where $\overline{J}$ is the current distribution over a strip and $\overline{\overline{G}}^p$ is the 2-D periodic dyadic Green's function. The details of deriving $\overline{\overline{G}}^p$ can be found in [8]. By enforcing the boundary conditions on the surface of the strip, that is, $\hat{y} \times (\overline{E}^i + \overline{E}^r) = -\hat{y} \times \overline{E}^s$, an integral equation for the unknown current distribution can be obtained. The electric field $\overline{E}^i$ refers to the incident plane wave and $\overline{E}^r$ refers to the field reflected from the stratified medium in the absence of the strips. The current can be

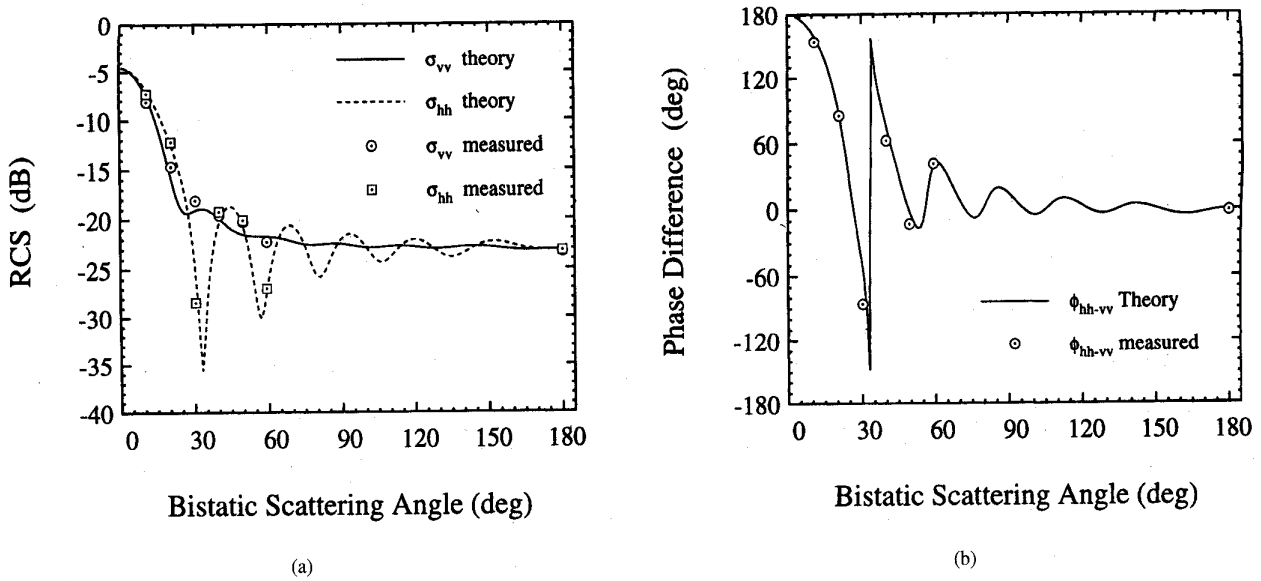

(a) (b)

Fig. 8. The magnitude (a) and phase-difference (b) of the bistatic scattering matrix elements of the 8.1 cm metallic sphere at 9.5 GHz.

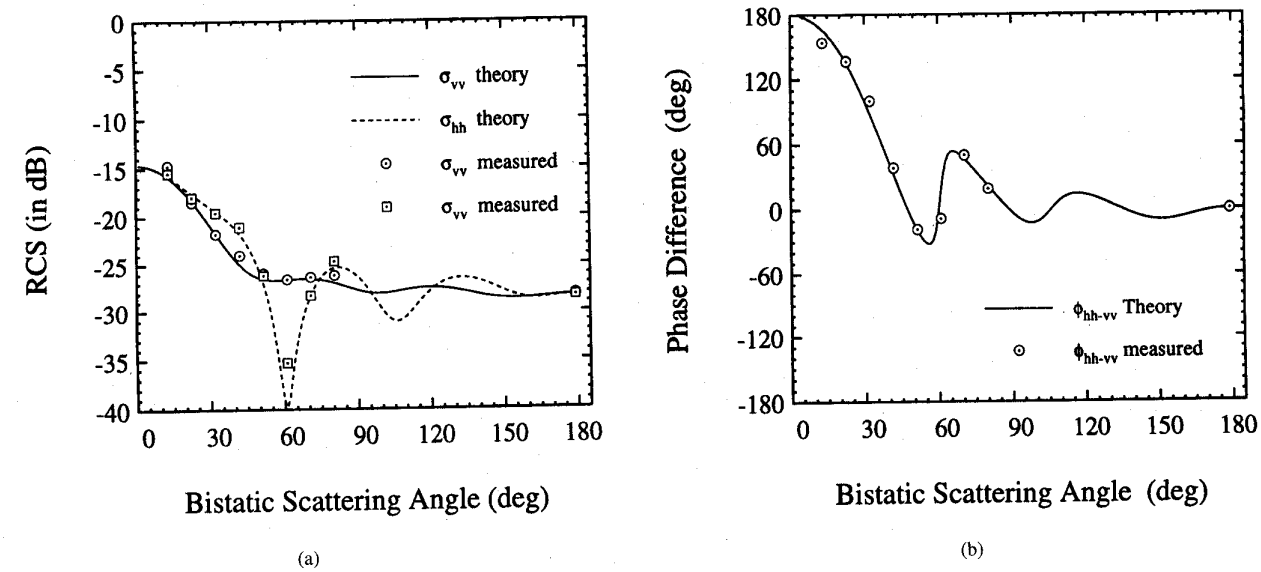

(a) (b)

Fig. 9. (a) The magnitude and (b) phase-difference of the bistatic scattering matrix elements of the 4.45 cm metallic sphere at 9.5 GHz.

computed by solving the integral equation using the method of moments. Once the surface current on the strip is determined, the scattered electric and magnetic fields, as well as the reflection coefficients for TE and TM polarizations can be computed from

$$\Gamma_E = \frac{E_z^r + E_z^s}{E_z^i}, \qquad \Gamma_H = \frac{H_z^r + H_z^s}{H_z^i} \tag{11}$$

where Γ_E and Γ_H are the reflection coefficients for TM and TE polarizations, respectively. As before, when $w < 0.5\lambda$ only the zeroth order Bragg mode is propagating. The phases of Γ_E and Γ_H of the dielectric loaded periodic strips are shown in Fig. 6(b) at 9.5 GHz when $d = w = 0.1\lambda$ and $\epsilon = 2.5$.

V. Experimental Verification

To demonstrate the accuracy of the new bistatic measurement technique, the measured bistatic responses of three canonical targets (two metallic spheres with different diameters and a tilted metallic cylinder) are compared with their theoretical bistatic responses. A network analyzer-based, polarimetric, monostatic radar was used in these measurements [9]. The radar operates at 9.5 GHz with a 1.5 GHz bandwidth which corresponds to a spatial resolution of about 10 cm. A perfectly conducting circular disc with diameter 1.2 m was used as the ground plane. The ground plane was positioned inside the anechoic chamber at a distance $r = 15$ m away from the radar system and the target was located at $\beta = 45°$ and $d_t = 0.6$ m,

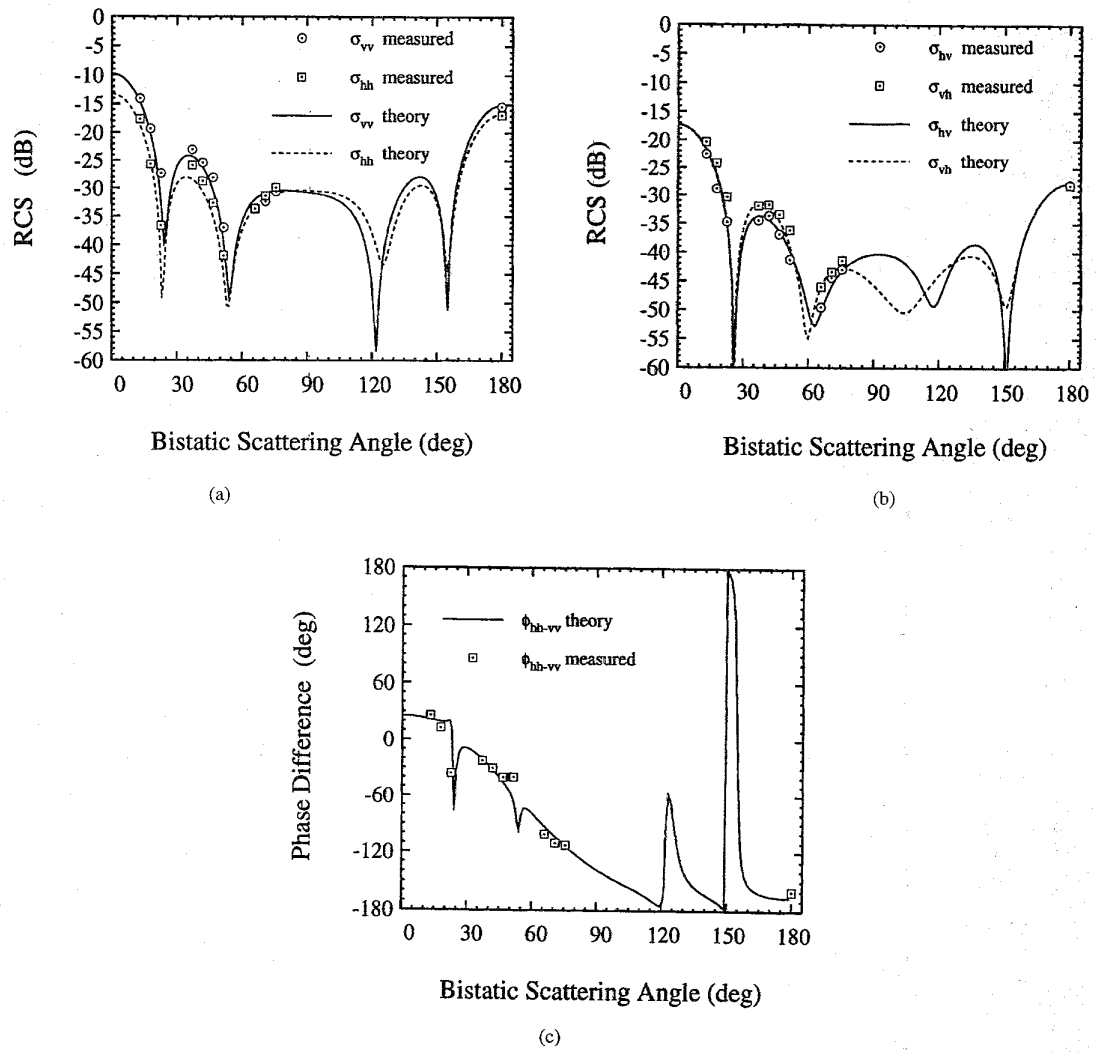

Fig. 10. (a) The magnitude, (b) the magnitude, and (c) phase-difference of the bistatic scattering matrix elements of a tilted (30° from vertical) metallic cylinder with length 15 cm and diameter 1.5 cm at 9.5 GHz.

with respect to the ground plane as depicted in Figs. 2 and 3. The ground plane was aligned with the radar using a laser system and by maximizing its radar return at normal incidence. Precise rotation of the ground plane was facilitated using a computer-controlled stepper motor. To characterize the system distortion parameters of the radar system, polarimetric measurements of a metallic sphere (without a ground plane) were conducted over the entire main lobe of the antenna system. The measured backscatter response of the sphere for the X-band radar is shown in Fig. 7 in an azimuth-over-elevation coordinate system (γ, ξ).

Two metallic spheres with diameters 4.45 cm and 8.1 cm were measured and compared with their theoretical responses over a number of bistatic angles including the backscatter direction to demonstrate the capability of the calibration technique in removing the systematic errors. As mentioned before, the spurious responses of the finite ground plane were removed by subtracting the backscatter response of the ground plane in the absence of the target from that of the combination of the target and the ground plane. Figs. 8 and 9 show the measured and computed bistatic radar cross sections (σ_{vv} and σ_{hh}) and the copolarized phase difference (ϕ_{hh-vv}) of the 4.45 cm and 8.1 cm spheres, respectively. The measured bistatic radar cross sections and phase differences, for both spheres, were, respectively, within ±0.5 dB and ±5° of the theoretical computations.

Spheres are nondepolarizing targets and in their measurments the anisotropic dielectric layer was not used. Next, the bistatic scattering matrix of a tilted metallic cylinder was measured to demonstrate the accuracy and feasibility of measuring the cross-polarized components of the scattering matrix. The length and diameter of the metallic cylinder were 15 cm and 1.5 cm, respectively. The cylinder was positioned in a plane perpendicular to the direction of propagation of the incident wave with a tilt angle of 30°, with respect to the vertical direction. A set of measurements were conducted first with

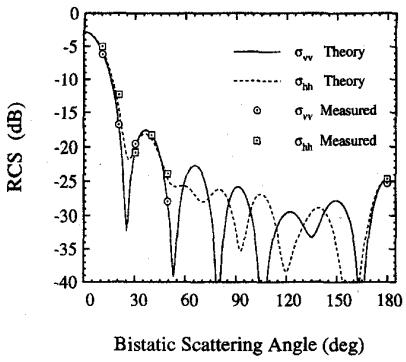

(a)

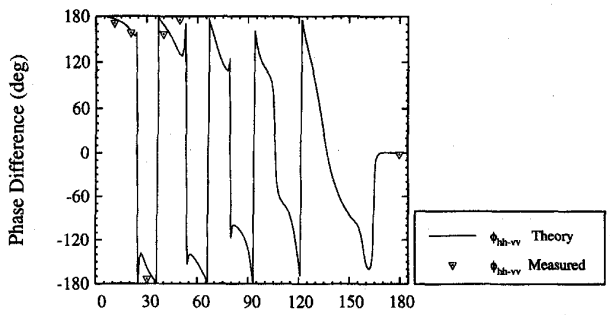

(b)

Fig. 11. The average magnitude (a) and the average phase-difference (b) of the copolarized bistatic scattering matrix elements of the collection of sand particles confined in a sphere with radius 3.87 cm measured at 9.5 GHZ.

the perfectly conducting plane as the reflecting surface. Then, the measurements were repeated after overlaying the dielectric loaded periodic strips (DLPS) slab on the ground plane. The DLPS slab was oriented so that its strips were aligned along the vertical direction. The phases of the reflection coefficients of the DLPS slab were computed from the method of moments solution and used in the calibration procedure. The method of moments phase calculation for the reflection coefficients was verified experimentally by measuring the phase difference between the reflection coefficients of the vertical and horizontal polarizations at normal incidence. The bistatic scattering matrix of the tilted cylinder was computed numerically using the method of moments specialized for scatterers with axial symmetry (body of revolution) [10]. As shown in Fig. 10, excellent agreement was obtained between the theoretically computed and the measured bistatic cross sections ($\sigma_{vv}, \sigma_{hh}, \sigma_{hv}$, and σ_{vh}) and the copolarized phase difference (ϕ_{hh-vv}) of the tilted cylinder.

After building confidence in the ability of the new technique through measuring the bistatic scattering matrix of point targets, an attempt was made to estimate the effective dielectric constant of a dense random medium. For this purpose, bistatic measurements were performed on a collection of silica particles with mean diameter of 2 mm and volume fraction of 0.6 confined in a spherical boundary with average diameter of 7.74 cm. A computer controlled servomotor was used to rotate a styrofoam pedestal holding the spherical collection of random particles. Overall, 100 independent samples were collected for each bistatic scattering angle. The bistatic responses were calibrated following the procedure outlined in Section III and the coherent components of the scattered waves (mean fields) were extracted by averaging coherently the scattered fields of all independent samples. The bistatic scattering cross sections (σ_{vv} and σ_{hh}) and the phase difference (ϕ_{hh-vv}), derived from the measured mean fields, are shown in Fig. 11. These data are then used to fit the bistatic scattering response of a homogeneous dielectric sphere in order to characterize the effective dielectric constant of the dense random medium. In this process, the conjugate gradient optimization technique [11] was used to minimize the difference between the measured and the theoretical responses. Using the real and imaginary parts of ϵ_{eff} as free parameters, the following error function was defined and minimized

$$E = \sum_{i=1}^{N} \left[\left(\frac{\sigma_{vv}^m(i) - \sigma_{vv}^t(i)}{\sigma_{vv}^m(i)} \right)^2 + \left(\frac{\sigma_{hh}^m(i) - \sigma_{hh}^t(i)}{\sigma_{hh}^m(i)} \right)^2 + \left(\frac{\phi_{hh-vv}^m(i) - \phi_{hh-vv}^t(i)}{\phi_{hh-vv}^m(i)} \right)^2 \right] \tag{12}$$

where superscripts m and t refer to measured and theoretical responses, respectively. The best fit was achieved for $\epsilon_{eff} = 3.113 + j0.125$ and the results are shown in Fig. 11. The real part of the estimated ϵ_{eff} is higher than the value estimated from the dielectric mixing formulas for a mixture of silica particles and air. This can be attributed, in part, to the presence of glue that holds the particles together. A hollow spherical or cylindrical shell made up of styrofoam can be used in future measurements.

VI. Conclusion

A convenient technique for the bistatic scattering measurement of point targets was developed. In this technique, a monostatic radar with fine spatial resolution in conjunction with a rotatable ground plane was used to measure the bistatic scattering matrix. The new technique circumvents some limiting aspects of the traditional measurement technique. For example, since the transmitter, receiver, and the target are stationary, retaining the phase-coherence is no longer a problem (no moving cables) and a very accurate calibration can be performed. Also, construction of a complicated bistatic measurement setup for supporting and positioning the transmit and receive antennas, with respect to the target, is avoided. It was shown that for depolarizing targets, an independent radar measurement after loading the ground plane with a dielectric slab is required for determining the cross-polarized components of the bistatic scattering matrix. The accuracy of the new method was demonstrated by comparing the measured bistatic scattering matrices of cylinders and spheres with the theoretical ones over a wide range of scattering angles. Also, the application of this technique in estimating

the effective dielectric constant of a dense random medium was demonstrated.

REFERENCES

[1] R. D. De Roo and F. T. Ulaby, "Bistatic specular Scattering from rough dielectric surfaces," *IEEE Trans. Antennas Propagat.*, vol. 42, no. 2, pp. 220–231, Feb. 1994.

[2] T. B. A. Senior, K. Sarabandi, and F. T. Ulaby, "Measuring and modeling the backscattering cross section of a leaf," *Radio Sci.*, vol. 22, no. 6, pp. 1109–1116, Nov. 1987.

[3] ——,"Effect of curvature on the backscattering from a leaf," *J. Electron. Waves Appl.*, vol. 2, no. 7, pp. 653–670, 1988.

[4] L. Tsang, J. A. Kong, and R. T. Shin, *Theory of Microwave Remote Sensing*. New York: Wiley, 1985.

[5] P. F. Polatin, K. Sarabandi, and F. T. Ulaby, "Monte Carlo simulation of electromagnetic scattering from a heterogeneous two-component medium," *IEEE Trans. Antennas Propagat.*, vol. 43, no. 10, pp. 1048–1057, Oct. 1995.

[6] K. Sarabandi and F. T. Ulaby, "A convenient technique for polarimetric calibration of radar systems," *IEEE Trans. Geosci. Remote Sensing*, vol. 28, no. 6, pp. 1022–1033, Nov. 1990.

[7] K. Sarabandi, "Simulation of a periodic dielectric corrugation with an equivalent anisotropic layer," *Int. J. Infra. Millimeter Waves*, vol. 11, no. 11, pp. 1303–1321, Nov. 1990.

[8] ——, "Electromagnetic scattering from vegetation canopies," Ph.D. dissertation, Univ. Michigan, Ann Arbor, MI, 1989.

[9] M. A. Tassoudji, K. Sarabandi, and F. T. Ulaby, "Design consideration and implementation of the LCX polarimetric scatterometer (POLARSCAT)," Univ. Michigan, Ann Arbor, MI, Radiation Lab. Tech. Rep. 022486-4-T, June 1989.

[10] J. R. Mautz and R. F. Harrington, "Radiation and scattering from bodies of revolution," *Appl. Sci. Res.*, vol. 20, p. 405, 1969.

[11] W. H. Press, S. A. Teukolsky, W. T. Vetterling, and B. P. Flannery, *Numerical Recipes in FORTRAN: The Art of Scientific Computing*, 2nd ed. Cambridge: Cambridge Univ. Press, 1992.

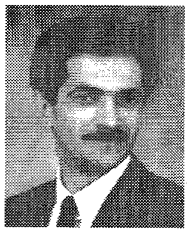

Kamal Sarabandi (S'87–M'90–SM'92) received the B.S. degree in electrical engineering from Sharif University of Technology, Tehran, Iran, in 1980. He entered the graduate program at the University of Michigan, Ann Arbor, MI, in 1984, and received the M.S.E. degree in electrical engineering in 1986, the M.S. degree in mathematics, and the Ph.D. degree in electrical engineering, in 1989.

From 1980–1984 he worked as a Microwave Engineer in the Telecommunication Research Center in Iran. He is presently an Assistant Professor in the Department of Electrical Engineering and Computer Science at the University of Michigan. He has 15 years of experience with microwave sensors and radar systems. In the past six years, he has served as principal investigator and co-investigator on many projects sponsored by NASA, JPL, ARO, DARPA, etc., all related in one way or the other to the radar remote sensing of environment.

Dr. Sarabandi has published four book chapters and more than 50 papers in refereed journals on electromagnetic scattering, random media modeling, microwave measurement techniques, radar calibration, application of neural networks in inverse scattering problems, and microwave sensors. He has also had more than 80 papers and presentations in national and international conferences and symposia on similar subjects. He is listed in *Who's Who in Electromagnetics* and is the chairman of the Geoscience and Remote Sensing Society, Southeast Michigan chapter.

Adib Nashashibi (S'82–M'95) received the B.Sc. and M.Sc. degrees in electrical engineering from Kuwait University, Kuwait, in 1985 and 1988, respectively. He received the Ph.D. degree in electrical engineering from the University of Michigan, Ann Arbor, in 1995.

Currently, he is a research fellow at the Radiation Laboratory at the University of Michigan. His research interests include microwave and remote sensing, polarimetric millimeter-wave radars, calibration and measurement techniques, wave propagation, and electromagnetic scattering from dense random media.